Single crystalline electronic structure and growth mechanism of aligned square graphene sheets

H. F. Yang, C. Chen, H. Wang, Z. K. Liu, T. Zhang, H. Peng, N. B. M. Schröter, S. A. Ekahana, J. Jiang, L. X. Yang, V. Kandyba, A. Barinov, C. Y. Chen, J. Avila, M. C. Asensio, H. L. Peng, Z. F. Liu, and Y. L. Chen

Citation: APL Materials **6**, 036107 (2018); doi: 10.1063/1.5012947

View online: https://doi.org/10.1063/1.5012947

View Table of Contents: http://aip.scitation.org/toc/apm/6/3

Published by the American Institute of Physics

Single crystalline electronic structure and growth mechanism of aligned square graphene sheets

H. F. Yang,[1,2,3,4,a] C. Chen,[2,a] H. Wang,[5,a] Z. K. Liu,[3,4,a] T. Zhang,[2,6] H. Peng,[2] N. B. M. Schröter,[2] S. A. Ekahana,[2] J. Jiang,[4] L. X. Yang,[6] V. Kandyba,[7] A. Barinov,[7] C. Y. Chen,[8] J. Avila,[8] M. C. Asensio,[8] H. L. Peng,[5,b] Z. F. Liu,[5,b] and Y. L. Chen[2,3,4,6,b]

[1]*State Key Laboratory of Functional Materials for Informatics, Shanghai Institute of Microsystem and Information Technology, Chinese Academy of Sciences, Shanghai 200050, People's Republic of China*
[2]*Clarendon Laboratory, Department of Physics, University of Oxford, Oxford OX1 3PU, United Kingdom*
[3]*CAS-Shanghai Science Research Center, Shanghai 201203, People's Republic of China*
[4]*School of Physical Science and Technology, ShanghaiTech University, Shanghai 200031, People's Republic of China*
[5]*Center for Nanochemistry, Beijing National Laboratory for Molecular Sciences, State Key Laboratory for Structural Chemistry of Unstable and Stable Species, College of Chemistry and Molecular Engineering, Peking University, Beijing 100871, People's Republic of China*
[6]*State Key Laboratory of Low Dimensional Quantum Physics, Collaborative Innovation Center of Quantum Matter and Department of Physics, Tsinghua University, Beijing 100084, China*
[7]*Elettra-Sincrotrone Trieste ScPA, Trieste, Basovizza 34149, Italy*
[8]*SOLEIL, L'Orme des Merisiers, Saint Aubin-BP 48, 91192 Gif sur Yvette Cedex, France*

(Received 9 November 2017; accepted 21 February 2018; published online 30 March 2018)

Recently, commercially available copper foil has become an efficient and inexpensive catalytic substrate for scalable growth of large-area graphene films for fundamental research and applications. Interestingly, despite its hexagonal honeycomb lattice, graphene can be grown into large aligned square-shaped sheets on copper foils. Here, by applying angle-resolved photoemission spectroscopy with submicron spatial resolution (micro-ARPES) to study the three-dimensional electronic structures of square graphene sheets grown on copper foils, we verified the high quality of individual square graphene sheets as well as their merged regions (with aligned orientation). Furthermore, by simultaneously measuring the graphene sheets and their substrate copper foil, we not only established the (001) copper surface structure but also discovered that the square graphene sheets' sides align with the ⟨110⟩ copper direction, suggesting an important role of copper substrate in the growth of square graphene sheets—which will help the development of effective methods to synthesize high-quality large-size regularly shaped graphene sheets for future applications. This work also demonstrates the effectiveness of micro-ARPES in exploring low-dimensional materials down to atomic thickness and sub-micron lateral size (e.g., besides graphene, it can also be applied to transition metal dichalcogenides and various van der Waals heterostructures) https://doi.org/10.1063/1.5012947

Graphene, a unique single-layer carbon sheet with a honeycomb lattice, has attracted enormous research interests in the past decade due to its elegant structural and electronic properties as well as great potentials in applications.[1–5] Recently, chemical vapour deposition (CVD) has emerged as a promising, efficient, and inexpensive method to realize scalable production of large-scale graphene

[a]H. F. Yang, C. Chen, H. Wang, and Z. K. Liu contributed equally to this work.
[b]Authors to whom correspondence should be addressed: hlpeng@pku.edu.cn, zfliu@pku.edu.cn, yulin.chen@physics.ox.ac.uk

films.[6,7] Nonetheless, the quality of such films has been suspected to be inferior to the exfoliated thin films due to defects during growth and boundaries between different graphene domains.[8–12] Such inhomogeneity not only adversely affected device applications but also made the conventional angle-resolved photoemission spectroscopy (ARPES) a powerful tool for the study of electronic structures[13–15] unsuitable for studying CVD thin films, as which typically is composed of single-crystalline individual and merged graphene grains of tens of micro-meters, much smaller than the conventional ARPES photon beam spot size (usually 0.5–1.0 mm). Consequently, conventional ARPES will only give the averaged band structure from many individual graphene grains with various crystalline orientations.

Recently, the situation has been greatly improved from both aspects. On one hand, the development of ARPES with very high (e.g., sub-micron) spatial resolution (i.e., micro-ARPES) in the past few years[16–18] provides a new powerful tool to directly probe the electronic structures of low-dimensional materials down to atomic thickness and sub-micrometer lateral size,[19–22] which enables us to investigate individual graphene grains and merged regions as well as the inhomogeneity of these films and gain valuable information about growth mechanism. On the other hand, low-pressure CVD growth methods[23,24] were developed and oxygen was introduced to reduce the nucleation density and increase the quality of graphene grains as well as the growth rate.[25–27] Interestingly, besides the usual hexagonal shape, graphene can also be grown into large aligned square-shape grains, despite its hexagonal honeycomb lattice.[28–30] If the orientations of such individual graphene grains can be aligned to enable seamless merging and then form a larger sheet, the quality of the CVD graphene films can be further improved.[31,32] Under this circumstance, an effective method that can investigate the electronic structures of these graphene films with precise spatial information and study their inhomogeneity is urgently needed.

In this work, we applied micro-ARPES to study the electronic structures and lattice orientation of square graphene grains grown on commercially available Cu foil substrate, as well as their growth mechanism. Taking advantage of the excellent spatial resolution of micro-ARPES, we were able to measure individual square graphene grains (and even different locations within one grain) to set up a direct link between the square grains' geometric shape and their lattice orientation. Furthermore, with the capability of simultaneously collecting photoelectrons from both graphene grains and the Cu substrate underneath, we could study their electronic structures and investigate their correspondence, which can shed light on the growth mechanism that results in their high quality and unusual square shape.

Figure 1(c) shows the principle of micro-ARPES technique. Complementary to other commonly used characterization methods [e.g., low energy electron diffraction (LEED), Raman, and transmission electron microscope (TEM)], micro-ARPES can directly visualize the electronic band structures of individual graphene grains and study their uniformity, as well as the grain-to-grain evolution with submicron spatial resolution. Furthermore, given the advantage that photoelectrons from both graphene and substrate Cu foil can be simultaneously collected and analyzed [see Fig. 1(c) and the supplementary material for details], the correlation between electronic structures of graphene grains and the Cu substrate can be investigated, leading to important information for understanding the growth mechanism. In addition, as a surface sensitive probe (supplementary material), micro-ARPES can provide information about what happened to topmost layers of Cu substrate which are directly involved in the CVD growth (instead of the bulk counterpart).

The square graphene grains in our study were grown on Cu foils by a low-pressure CVD method at a high growth rate (the maximum can reach 300 μm min^{-1}).[30] In particular, two Cu foils were stacking together (with a gap of around tens of microns) and inside molecular move in a molecular-flow-mode[30] [Fig. 1(b)]. From the optical image [Fig. 1(a)], individual graphene square grains can be easily identified and some of them even merge to form larger sheets (up to millimeter scale). The larger size and the smoother sides of individual square graphene grains from our synthesis[30] show the improvement over some previous studies that typically yield smaller grains with jagged edges.[28,29]

In order to investigate both individual graphene grains and their merged regions, we chose an area marked by the orange rectangle in Fig. 1(a) (optical image). The corresponding photoemission intensity map in real space obtained by micro-ARPES is illustrated in Fig. 1(d), showing excellent correspondence to Fig. 1(a).

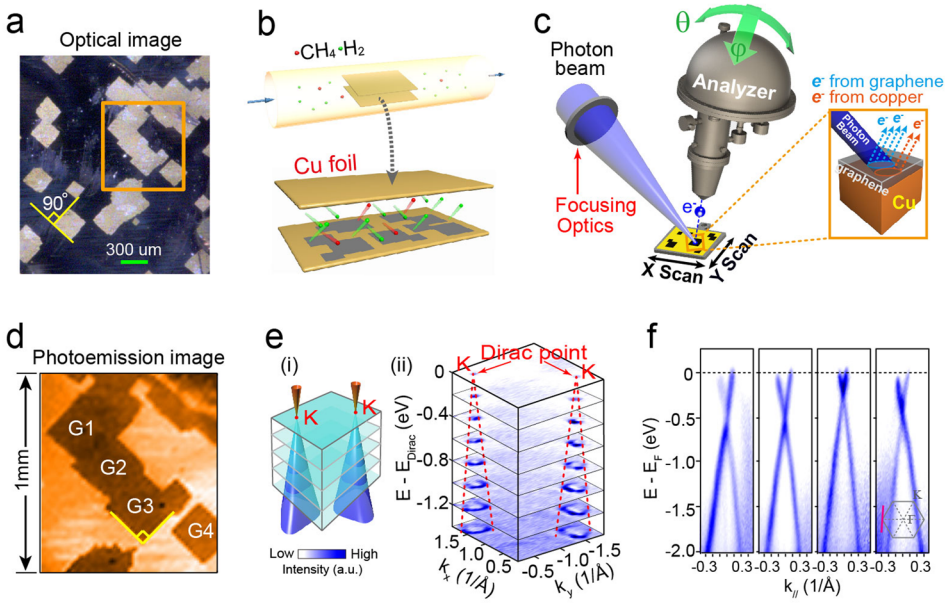

FIG. 1. General characterizations of square graphene and brief introduction to micro-ARPES. (a) Optical image of well-aligned square graphene sheets. (b) Schematic of CVD growth of square graphene sheets. (c) Schematic of micro-ARPES. Because of the focusing optics delicately designed, the beam size is reduced to sub-micron size, thus significantly adding the spatial resolution to ARPES (more details about micro-ARPES can be found in the supplementary material). In the photoemission process, photoelectrons from both graphene and Cu substrate can be detected simultaneously since the thickness of graphene sheets is smaller than the penetration depth of photoelectrons probed in our experiments. (d) Micro-ARPES real-space map of square graphene sheets. This region corresponds to the orange rectangular region in (a). (e) Schematic illustration (left panel) and measured (right panel) characteristic Dirac cones of single-layer graphene from grain G2 (only two Dirac cones are shown), exhibiting the single-layer nature. To display the Dirac point and dispersion clearly, only the lower part of the Dirac cone is presented. The blurry features arise from the Cu *sp* band. (f) Photoemission spectra acquired at four different positions of square graphene sheets (see Fig. S3 of the supplementary material) all exhibit robust linear band dispersions of Dirac cones and reveal electron-doped nature of graphene on Cu.

In order to check if each square graphene grain is single layer and single crystalline, we first focused the photon beam onto different grains to measure their band dispersions in momentum space, which can be compared with the theoretical band structure of mono-layer graphene as schematically shown in Fig. 1(e–i). Indeed, the measurement in Fig. 1(e–ii) [stacking plot of constant energy contours of the photoemission spectral intensity from grain G2 in Fig. 1(d)] shows excellent agreement with that in Fig. 1(e–i). Besides the constant energy contours, we can also obtain band dispersions across the Dirac points from different grains, as shown in Fig. 1(f). All grains exhibit clear single linear dispersions around the *K* point in momentum space, indicating the single-layer and electron-doped nature of these grains [note that the variation of doping level at different positions can be mainly ascribed to the local Cu-graphene separation variation (considering the corrugated nature of Cu foil, Fig. S1 of the supplementary material) that influences the extent of charge transfer and doping level[21,33]].

Interestingly, as these square graphene grains are apparently well-aligned [their sides are parallel aligned; Figs. 1(a) and 1(d)], we can compare the band structures of different grains and their merged region to check if this is indeed the case (lattice structures are aligned). Figure 2 summarizes various measurements on graphene grains from two different samples labeled as Sample A and Sample B (from different growth batches). The real-space spectral intensity maps of Sample A and B are displayed in Figs. 2(a) and 2(e), respectively, while the constant energy contours cutting through the Dirac points in momentum space are shown in Figs. 2(b) and 2(f), respectively. Evidently, from each graphene domain, only a single set of Dirac points are observed [Figs. 2(b) and 2(f)] as expected [Fig. 2(d)], again proving their single-layer nature.

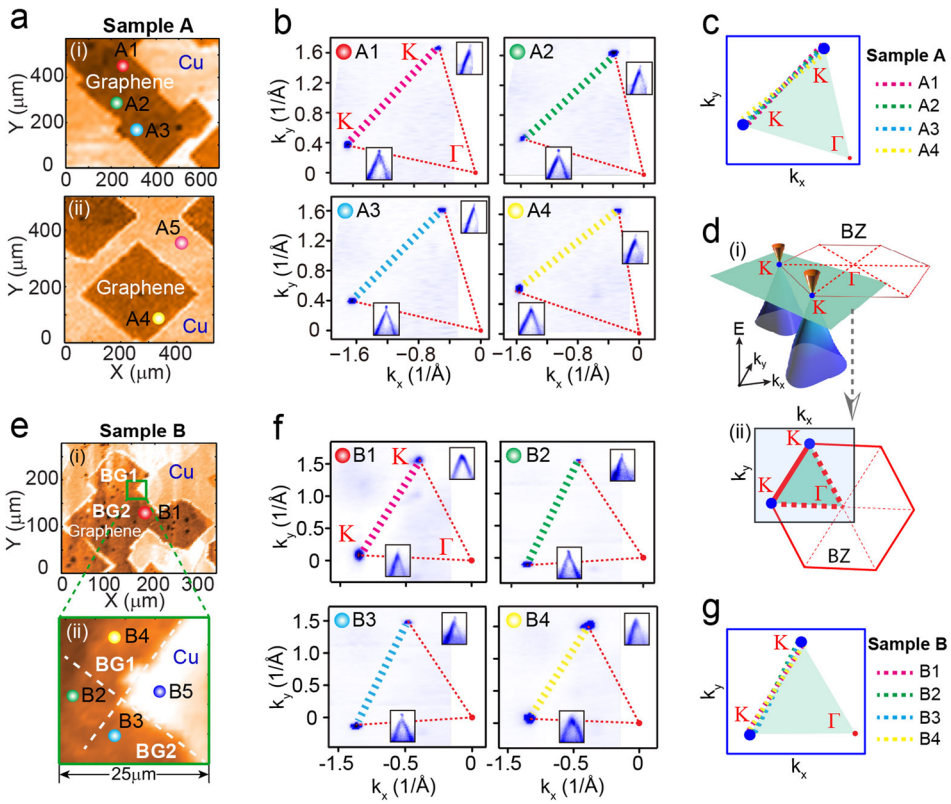

FIG. 2. Highly aligned orientation of single-layer square graphene grains. (a) 2D real-space maps of Sample A. Overlaid colored spheres represent the positions (A1-A5) we have probed (note that A5 is the bare Cu). (b) Constant energy contours (crossing the Dirac points in the momentum space) measured at different positions (A1–A4) of graphene sheets in Sample A. The insets display Dirac band dispersions cutting through the Dirac points. (c) All measured K–K directions (connecting the two measured Dirac points) are plotted together. They are all approximately parallel aligned (considering the substrate corrugation and experimental uncertainty). (d) Schematic of Dirac cones of single-layer graphene (i) and constant energy contour crossing the Dirac points (ii). [(e)–(g)] The same as (a)–(c) but for Sample B. Our data reveal that grains in Sample B are single layer and approximately parallel aligned.

Remarkably, in Fig. 2(b) or Fig. 2(f), one can easily find that the measurements from different grains of the same sample are almost identical in momentum space, which can be verified by overlapping these measurements for comparison [see Fig. 2(c) for Sample A and Fig. 2(g) for Sample B]. The slight variation of the Dirac point positions in Figs. 2(c) and 2(g) is due to the experimental uncertainty resulting from the surface unevenness of the Cu foil (corrugation is common in commercial Cu foils used in CVD growth; see Fig. S1 of the supplementary material) and the angle variation due to the rotation of the electron analyzer of micro-ARPES. Since the orientation of the band structure in momentum space is reciprocal to the lattice orientation in real space [see Fig. S7(a) and S7(b) in the supplementary material for details], the good agreement of the band structures [Figs. 2(c) and 2(g)] shows that the lattice orientation of different graphene grains in each sample is also well aligned, which is consistent with reported selected-area electron diffraction measurements.[30]

Besides the individual grains, we find that the merged regions between different grains also show high crystalline quality with the same lattice orientation as individual grains. As examples, measurements at points A1 [in Sample A, see Fig. 2(a)] and B2 residing at the merged area of two graphene grains BG1 and BG2 [in Sample B, see Fig. 2(e–ii)], both show matched orientation to their neighboring grains. This observation suggests that the individual graphene grains can merge into a larger sheet with similar crystalline orientation, making our CVD growth a promising method to grow large-scale graphene sheets with high quality.

After establishing that the square-shaped grains are indeed single-layer graphene sheets with aligned orientation, we can further investigate if and how their electronic structures, shape, and lattice orientation are related to those of the Cu foil underneath, which may help understand the role of the Cu substrate in the CVD growth that is still under debate.[34–41]

We first measured the electronic and lattice structures of bare Cu foil by focusing the photon beam to the Cu substrate next to the graphene grain under investigation [Fig. 3(a)]. The constant energy contour of the Cu *d* band [Fig. 3(b)] clearly shows four-fold symmetry with the periodicity (~2.5 $Å^{-1}$) consistent with the Cu (001) surface. We then moved the photon beam to the adjacent graphene grain [see Fig. 3(c–i)] where we can simultaneously measure the band structures of graphene and Cu substrate. The results on graphene covered regions of both Samples A and B are displayed in Fig. 3(d). In addition to the square-shaped band contours (from the Cu substrate) shown in Fig. 3(b),

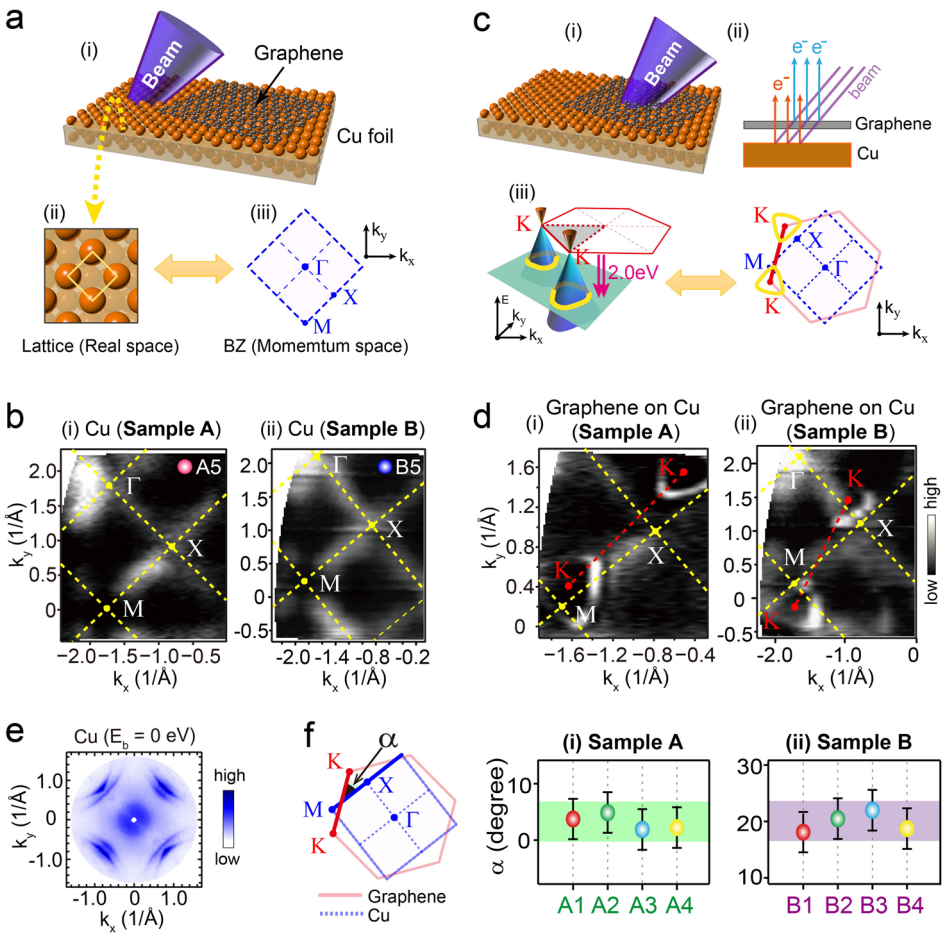

FIG. 3. Alignment relation between graphene grains and Cu substrate in momentum space. (a) Schematic of the Cu (001) surface (i) with a top-view image (ii). In (iii), the BZ of Cu (001) surface is presented (to label the high-symmetry points in a simple way, the Cu substrate is treated as two-dimensional square lattice, given that only topmost layers of Cu are measured by micro-ARPES and involved in the growth). (b) Constant energy (E_B − 2.3 eV) contours of bare Cu: A5 and B5 are from Sample A (i) and B5 (ii), respectively. Four-fold cross-like bands are Cu *d* band. [(c) and (d)] The same as (a) and (b), but the focus is on the graphene region; thus, band structures of graphene and copper underneath were simultaneously measured. In (d), apart from the Cu (*d*) band, two robust triangle-like bands are "footprints" of Dirac cones from graphene. (e) Mirror-symmetrized Fermi surface of the Cu substrate stemming from the *sp* band measured at the ANTARES beamline with unfocused photon beam (photon beam size > 50 μm) and high instrumental resolutions. In this measurement, 100 eV photons were used to enhance the Cu *sp* band. It clearly shows four-fold symmetry (see Fig. S6 and the supplementary material for details). (f) Negligible position dependence of α (defined as the angle between the *K*–*K* direction of graphene and the *X*–*M* direction of Cu substrate) within one sample (Sample A or B). Note that an error bar of ±3° is applied, considering the wrinkled nature of Cu foils and graphene grains (see Fig. S1 of the supplementary material) and instrumental resolutions.

Fig. 3(d) clearly shows additional triangular band contours centered at the *K* points from the Dirac cone of the graphene grains. In order to further check the uniformity of the Cu substrate, an unfocused photon beam (>50 μm beam spot size) was used [see Fig. 3(e); 100 eV photons were used to enhance the Cu *sp* band near E_F]. Remarkably, the sharp single-domain Fermi-surface in Fig. 3(e) (also see Fig. S6 in the supplementary material for more details) with four-fold symmetry clearly demonstrates the single crystalline nature of the Cu (001) substrate in a large area that was also confirmed by electron back-scatter diffraction (EBSD) measurements.[30]

With both band structures from graphene grains and the Cu substrate, we can examine their relative orientation, which we define as the angle α [Fig. 3(f)] between the *K*–*K* direction of the graphene Brillouin zone (BZ) and the *X*–*M* direction of the Cu (001) BZ. Interestingly, after comparing different graphene grains from Samples A and B, we find that [Fig. 3(f)] although in each sample the α values are consistent for different graphene grains [considering the substrate corrugation (see Fig. S1 of the supplementary material) and experimental uncertainty], between different samples, α is clearly different [Fig. 3(f)] which indicates that the relative crystalline orientation between graphene grains and the Cu substrate may not be critical for the formation of the square graphene grains.

Instead, we now consider if the geometrical shape of the square grains in both samples is correlated to the Cu substrate. As the electronic structure's orientation in momentum space is reciprocal to the lattice orientation in real space, we can also investigate how the sides of the square grains

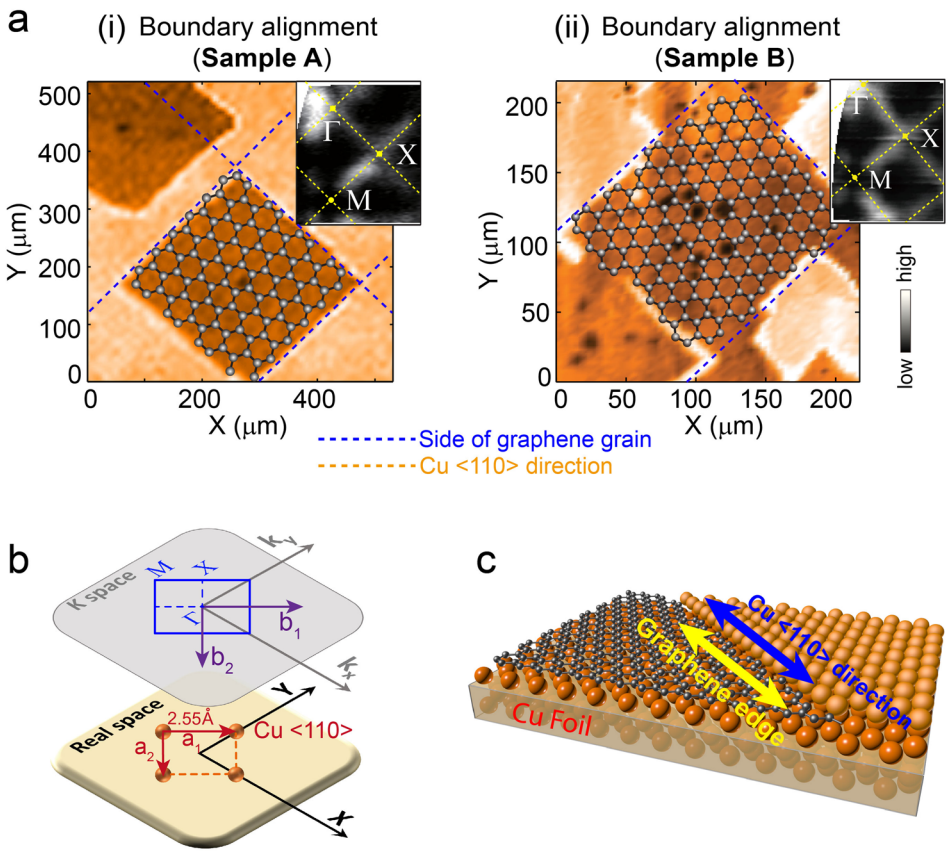

FIG. 4. Alignment relation between lattices and sides of graphene grain and lattices of Cu substrate. (a) Alignment relations of Samples A (i) and B (ii). The blue dashed lines represent the sides of the grains in the real-space maps; the inset shows the constant-energy contour and Cu BZ in momentum space, and the overlaid graphene lattices are reconstructed from the angle α determined in Fig. 3(d). (b) Schematic of the correspondence between momentum space and real space of Cu (001). The *X*–*M* direction is parallel to the Cu ⟨110⟩ lattice direction. (c) Sides of graphene grains of both samples are parallel aligned with respect to the ⟨110⟩ lattice direction of the underlying Cu. The side of graphene may extend along a possible Cu ⟨110⟩ step edge.

are aligned with the lattice directions of the Cu (001) surface underneath from the measurements in Fig. 3.

In Fig. 4, the reconstructed graphene lattice orientation, the geometrical grains' side orientation, and the high-symmetry directions in reciprocal space of the Cu (001) surface (with which lattice orientation of Cu can be deduced) are plotted together and then compared. Figure 4(a) shows that the zigzag and armchair edges are roughly aligned with the sides of the graphene grain in Sample A [panel (i)], while in Sample B [panel (ii)] they are clearly misaligned, again confirming our above discussions [the correspondence between the BZ in momentum space and the lattice in real space is illustrated in Figs. 4(b) and S7 in the supplementary material]. Despite this difference, in Fig. 4(a), both samples show that the sides of the graphene grains (blue dashed lines) determined from the real-space maps are significantly parallel to the *X*–*M* direction of the Cu substrate [i.e., the Cu ⟨110⟩ direction, marked as the yellow dashed lines in the insets of Figs. 4(a-i) and 4(a-ii)].

This correspondence in both samples suggests that certain Cu atomic direction plays an important role during the growth of the square graphene grains. Figure 4(c) shows a possible picture where graphene grains preferentially nucleate and extend along the Cu ⟨110⟩ step edge (since atomic steps on Cu foils were revealed by atomic force microscope measurements[30]). In this regard, the shape and orientation of graphene grains are highly influenced by the Cu (001) crystalline surface structure.

In summary, we successfully applied the state-of-the-art micro-ARPES technique in the systematic study of spatially resolved electronic structures of aligned square graphene sheets grown on commercially available Cu foil. We confirmed the graphene sheets' high quality and well-aligned orientation and furthermore revealed that the crystalline surface structure of Cu foils plays an essential role in the formation of their square shape during CVD growth. In addition, our work demonstrates the potential of this new experimental technique in the study of low-dimensional materials down to atomic thickness and sub-micrometer lateral size (e.g., besides graphene, it can also be applied to transition metal dichalcogenides,[42] various van der Waals heterostructures,[43] and black phosphorus[44]) and even *in situ* study of the active materials used in functional devices.

See supplementary material for detailed experimental description and data.

Y. L. Chen acknowledges the support from the EPSRC (UK) Grant No. EP/K04074X/1 and a DARPA (USA) MESO Project (No. N66001-11-1-4105). H. F. Yang acknowledges the financial support from the Bureau of Frontier Sciences and Education, Chinese Academy of Sciences. C. Chen and H. Peng acknowledge the support from China Scholarship Council—University of Oxford. S. A. Ekahana acknowledges the support from Indonesia Endowment Fund for Education (Lembaga Pengelolaan Dana Pendidikan, LPDP). N. B. M. Schröter acknowledges the support from Studienstiftung des deutschen Volkes.

[1] A. H. Castro Neto, F. Guinea, N. M. R. Peres, K. S. Novoselov, and A. K. Geim, Rev. Mod. Phys. **81**, 109 (2009).
[2] A. K. Geim, Science **324**, 1530–1534 (2009).
[3] R. Grantab, V. B. Shenoy, and R. S. Ruoff, Science **330**, 946–948 (2010).
[4] W. Han, R. K. Kawakami, M. Gmitra, and J. Fabian, Nat. Nanotechnol. **9**, 794–807 (2014).
[5] S. Bae, H. Kim, Y. B. Lee, X. F. Xu, J. S. Park, Y. Zheng, J. Balakrishnan, T. Lei, H. R. Kim, Y. I. Song, Y. J. Kim, K. S. Kim, B. Özyilmaz, J.-H. Ahn, B. H. Hong, and S. Iijima, Nat. Nanotechnol. **5**, 574–578 (2010).
[6] X. S. Li, W. Cai, J. An, S. Kim, J. Nah, D. X. Yang, R. Piner, A. Velamakanni, I. Jung, E. Tutuc, S. K. Banerjee, L. Colombo, and R. S. Ruoff, Science **324**, 1312–1314 (2009).
[7] C. Mattevi, H. Kim, and M. Chhowalla, J. Mater. Chem. **21**, 3324–3334 (2011).
[8] A. Mesaros, S. Papanikolaou, C. F. J. Flipse, D. Sadri, and J. Zaanen, Phys. Rev. B **82**, 205119 (2010).
[9] O. V. Yazyev and S. G. Louie, Nat. Mater. **9**, 806–809 (2010).
[10] Q. K. Yu, L. A. Jauregui, W. Wu, R. Colby, J. F. Tian, Z. H. Su, H. L. Cao, Z. H. Liu, D. Pandey, D. G. Wei, T. F. Chung, P. Peng, N. P. Guisinger, E. A. Stach, J. M. Bao, S.-S. Pei, and Y. P. Chen, Nat. Mater. **10**, 443–449 (2011).
[11] D. W. Kim, Y. H. Kim, H. S. Jeong, and H. T. Jung, Nat. Nanotechnol. **7**, 29–34 (2012).
[12] A. W. Tsen, L. Brown, M. P. Levendorf, F. Ghahari, P. Y. Huang, R. W. Havener, C. S. Ruiz-Vargas, D. A. Muller, P. Kim, and J. Park, Science **336**, 1143–1146 (2012).
[13] A. Damascelli, Z. Hussain, and Z. X. Shen, Rev. Mod. Phys. **75**, 473 (2003).
[14] D. H. Lu, I. M. Vishik, M. Yi, Y. L. Chen, R. G. Moore, and Z. X. Shen, Annu. Rev. Condens. Matter Phys. **3**, 129–167 (2012).
[15] Y. L. Chen, Front. Phys. **7**, 175–192 (2012).

[16] P. Dudin, P. Lacovig, C. Fava, E. Nicolini, A. Bianco, G. Cautero, and A. Barinov, J. Synchrotron Radiat. **17**, 445 (2010).
[17] J. Avila, I. Razado, S. Lorcy, R. Fleurier, E. Pichonat, D. Vignaud, X. Wallart, and M. C. Asenio, J. Phys.: Conf. Ser. **425**, 192023 (2013).
[18] A. Bostwick, E. Rotenberg, J. Avila, and M. C. Asensio, Synchrotron Radiat. News **25**, 19–25 (2012).
[19] J. Avila, I. Razado, S. Lorcy, R. Fleurier, E. Pichonat, D. Vignaud, X. Wallart, and M. C. Asensio, Sci. Rep. **3**, 2439 (2013).
[20] H. T. Yuan, Z. K. Liu, G. Xu, B. Zhou, S. F. Wu, D. Dumcenco, K. Yan, Y. Zhang, S. K. Mo, P. Dudin, V. Kandyba, M. Yablonskikh, A. Barinov, Z. X. Shen, S. C. Zhang, Y. S. Huang, X. D. Xu, Z. Hussain, H. H. Hwang, Y. Cui, and Y. L. Chen, Nano Lett. **16**, 4738–4745 (2016).
[21] H. Peng, N. B. M. Schröter, J. B. Yin, H. Wang, T. F. Chung, H. F. Yang, S. Ekahana, Z. K. Liu, J. Jiang, L. X. Yang, T. Zhang, C. Chen, H. Ni, A. Barinov, Y. P. Chen, Z. F. Liu, H. L. Peng, and Y. L. Chen, Adv. Mater. **29**, 1606741 (2017).
[22] N. R. Wilson, P. V. Nguyen, K. Seyler, P. Rivera, A. J. Marsden, Z. P. L. Laker, G. C. Constantinescu, V. Kandyba, A. Barinov, N. D. M. Hine, X. D. Xu, and D. H. Cobden, Sci. Adv. **3**, e1601832 (2017).
[23] X. S. Li, C. W. Magnuson, A. Venugopal, R. M. Tromp, J. B. Hannon, E. M. Vogel, L. Colombo, and R. S. Ruoff, J. Am. Chem. Soc. **133**, 2816–2819 (2011).
[24] B. Zhang, W. H. Lee, R. Piner, I. Kholmanov, Y. P. Wu, H. F. Li, H. X. Ji, and R. S. Ruoff, ACS Nano **6**, 2471–2476 (2012).
[25] T. R. Wu, X. F. Zhang, Q. H. Yuan, J. C. Xue, G. Y. Lu, Z. H. Liu, H. S. Wang, H. M. Wang, F. Ding, Q. K. Yu, X. M. Xie, and M. H. Jiang, Nat. Mater. **15**, 43–47 (2016).
[26] Y. F. Hao, M. S. Bharathi, L. Wang, Y. Y. Liu, H. Chen, S. Nie, X. H. Wang, H. Chou, C. Tan, B. Fallahazad, H. Ramanarayan, C. W. Magnuson, E. Tutuc, B. I. Yakobson, K. F. McCarty, Y. W. Zhang, P. Kim, J. Hone, L. Colombo, and R. S. Ruoff, Science **342**, 720–723 (2013).
[27] X. Z. Xu, Z. H. Zhang, L. Qiu, J. N. Zhuang, L. Zhang, H. Wang, C. N. Liao, H. D. Song, R. X. Qiao, P. Gao, Z. H. Hu, L. Liao, Z. M. Liao, D. P. Yu, E. G. Wang, F. Ding, H. L. Peng, and K. H. Liu, Nat. Nanotechnol. **11**, 930–935 (2016).
[28] G. P. Dai, M. H. Wu, D. K. Taylor, and K. Vinodgopal, Mater. Res. Lett. **1**, 67–76 (2013).
[29] H. Wang, G. Z. Wang, P. F. Bao, S. L. Yang, W. Zhu, X. Xie, and W. J. Zhang, J. Am. Chem. Soc. **134**, 3627–3630 (2012).
[30] H. Wang, X. Z. Xu, J. Y. Li, L. Lin, L. Z. Sun, X. Sun, S. L. Zhao, C. W. Tan, C. Chen, W. H. Dang, H. Y. Ren, J. C. Zhang, B. Deng, A. L. Koh, L. Liao, N. Kang, Y. L. Chen, H. Q. Xu, F. Ding, K. H. Liu, H. L. Peng, and Z. F. Liu, Adv. Mater. **28**, 8968–8974 (2016).
[31] J. H. Lee, E. K. Lee, W. J. Joo, Y. Jang, B. S. Kim, J. Y. Lim, S. H. Choi, S. J. Ahn, J. R. Ahn, M. H. Park, C. W. Yang, B. L. Choi, S. W. Hwang, and D. Whang, Science **344**, 286–289 (2014).
[32] L. Brown, E. B. Lochocki, J. Avila, C. J. Kim, Y. Ogawa, R. W. Havener, D. K. Kim, E. J. Monkman, D. E. Shai, H. I. Wei, M. P. Levendorf, M. C. Asensio, K. M. Shen, and J. Park, Nano Lett. **14**, 5706–5711 (2014).
[33] P. A. Khomyakov, G. Giovannetti, P. C. Rusu, G. Brocks, J. van den Brink, and P. J. Kelly, Phys. Rev. B **79**, 195425 (2009).
[34] H. Kim, C. Mattevi, M. R. Calvo, J. C. Oberg, L. Artiglia, S. Agnoli, C. F. Hirjibehedin, M. Chhowalla, and E. Saiz, ACS Nano **6**, 3614–3623 (2012).
[35] H. I. Rasool, E. B. Song, M. Mecklenburg, B. C. Regan, K. L. Wang, B. H. Weiller, and J. K. Gimzewski, J. Am. Chem. Soc. **133**, 12536–12543 (2011).
[36] Y. F. Zhang, T. Gao, Y. B. Gao, S. B. Xie, Q. Q. Ji, K. Yan, H. L. Peng, and Z. F. Liu, ACS Nano **5**, 4014–4022 (2011).
[37] X. Y. Zhang, Z. W. Xu, L. Hui, J. Xin, and F. Ding, J. Phys. Chem. Lett. **3**, 2822–2827 (2012).
[38] L. Liu, D. A. Siegel, W. Chen, P. Z. Liu, J. J. Guo, G. Duscher, C. Zhao, H. Wang, W. L. Wang, X. D. Bai, K. F. McCarty, Z. Y. Zhang, and G. Gu, Proc. Natl. Acad. Sci. U. S. A. **111**, 16670–16675 (2014).
[39] T. P. C. Klaver, S. E. Zhu, M. H. F. Sluiter, and G. C. A. M. Janssen, Carbon **82**, 538–547 (2015).
[40] P. Wu, W. H. Zhang, Z. Y. Li, and J. L. Yang, Small **10**, 2136–2150 (2014).
[41] J. Cho, L. Gao, J. Tian, H. Cao, W. Wu, Q. Yu, E. N. Yitamben, B. Fisher, J. R. Guest, Y. P. Chen, and N. P. Guisinger, ACS Nano **5**, 3607–3613 (2011).
[42] K. F. Mak, C. G. Lee, J. Hone, J. Shan, and T. F. Heinz, Phys. Rev. Lett. **105**, 136805 (2010).
[43] A. K. Geim and I. V. Grigorieva, Nature **499**, 419–425 (2013).
[44] L. K. Li, Y. J. Yu, G. J. Ye, Q. Q. Ge, X. D. Ou, H. Wu, D. L. Feng, X. H. Chen, and Y. B. Zhang, Nat. Nanotechnol. **9**, 372–377 (2014).